J. metamorphic Geol., 2004, **22,** 45–62 doi:10.1111/j.1525-1314.2004.00496.x

Diffusion creep and partial melting in high temperature mylonitic gneisses, Hope Valley shear zone, New England Appalachians, USA

S. R. GARLICK AND L. P. GROMET
Department of Geological Sciences, Brown University, Providence, RI 02912, USA (l_gromet@brown.edu)

ABSTRACT Field, petrographic, microstructural and isotopic studies of mylonitic gneisses and associated pegmatites along the Hope Valley shear zone in southern Rhode Island indicate that late Palaeozoic deformation (*c.* 275 Ma) in this zone occurred at very high temperatures (> 650 °C). High-energy cuspate/lobate phase boundary microstructures, a predominance of equant to sub-equant grains with low internal lattice strain, and mixed phase distributions indicate that diffusion creep was an important and possibly predominant deformation mechanism. Field and petrographic evidence are consistent with the presence of an intergranular melt phase during deformation, some of which collected into syntectonic pegmatites. Rb/Sr isotopic analyses of tightly sampled pegmatites and wall rocks confirm that the pegmatites were derived as partial melts of the immediately adjacent, isotopically heterogeneous mylonitic gneisses. The presence of syntectonic interstitial melts is inferred to have permitted a switch from dislocation creep to melt-enhanced diffusion creep as the dominant mechanism in these relatively coarse-grained mylonitic gneisses (200–500 μm syn-deformational grain size). A switch to diffusion creep would lead to significant weakening, and may explain why the Hope Valley shear zone evolved into a major regional tectonic boundary. This work identifies conditions under which diffusion creep operates in naturally deformed granitic rocks and illuminates the deformation processes involved in the development of a tectonic boundary between two distinct Late Proterozoic (Avalonian) basement terranes.

Key words: Appalachians; diffusion creep; mylonitic gneiss; partial melting; pegmatite.

INTRODUCTION

Mylonite zones represent a heterogeneous distribution of strain, requiring either a strain-weakening mechanism or an initial or induced competency contrast to permit localization. Mylonites in quartzo-feldspathic rocks most typically develop at intermediate metamorphic temperatures, generally 300 to 600 °C or greenschist to amphibolite grade. Under these conditions the grain-size dependency of strength for particular deformation mechanisms (e.g. recrystallization-accommodated dislocation creep in feldspar; Tullis & Yund, 1985) can lead to strain localization. Other processes, such as syn-deformational reaction (Stünitz & Tullis, 2001), can also result in strain weakening and lead to strain localization.

Quartzo-feldspathic mylonitic and ultramylonitic gneisses were examined from a segment of the Hope Valley shear zone in the Avalon zone of the southern New England Appalachians (O'Hara & Gromet, 1985). What drew our attention to these rocks is that they formed in a region of relatively high metamorphic grade, where most quartzo-feldspathic rocks of similar composition experienced a distributed regional 'gneissification' rather than forming localized shear zones. A distributed deformation is consistent with the relatively low strength of quartzo-feldspathic rocks at high metamorphic grades, where recovery processes are able to keep up with dislocation glide and strain occurs homogeneously under low differential stress. Therefore, we were curious about what mechanisms could cause the grain size reduction and the localization of strain in these mylonitic gneisses.

Field and microstructural observations and the isotopic systematics of mylonitic gneisses and associated pegmatites reported here provide evidence that a significant component of strain in this zone was accommodated by melt-enhanced diffusion creep. Evidence for diffusion creep in quartzo-feldspathic rocks in nature and in experimental studies is generally restricted to very fine grain sizes of 10 μm or less (e.g. Behrmann & Mainprice, 1987; Tullis, 1990; Stünitz & FitzGerald, 1993; Fliervoet *et al.*, 1997), but syn-deformational grain sizes in the mylonitic gneisses studied here range up to 500 μm. If our interpretations are correct, these mylonitic gneisses are one of a relatively small number of known examples where diffusion creep is believed to occur in rocks with such a coarse grain size. Further, evidence is provided that deformation in this zone was associated with a switch in dominant deformation mechanism from dislocation creep to diffusion creep, and that this switch may have been aided by or even dependent on the presence of intergranular melt. The resulting weakening is inferred

to have led to strain localization. Thus, the results of this study have important implications for the understanding of the evolution of the Hope Valley shear zone as a terrane boundary, and more generally, the influence of melt on the strength of naturally deformed crustal rocks.

REGIONAL GEOLOGICAL SETTING

The Late Proterozoic Avalonian basement of south-eastern New England can be divided into two distinct terranes, the Esmond-Dedham and the Hope Valley terranes (O'Hara & Gromet, 1985; Hermes *et al*., 1994; Fig. 1). The Esmond-Dedham terrane consists of Late Proterozoic to middle Palaeozoic rocks (Hermes & Zartman, 1985), including the Late Proterozoic Ponaganset granitic augen gneiss and the Devonian Scituate granite gneiss of western and central Rhode Island. The Hope Valley terrane contains Late Proterozoic Hope Valley alaskite and other gneisses (Hermes & Zartman, 1985) and intrusions of the Permian Narragansett Pier granite, but no rocks of middle Palaeozoic age. A zone of highly deformed gneisses is developed along the tectonic contact between these two terranes (the Hope Valley shear zone of O'Hara & Gromet, 1985), stretching 60–70 km from around Northbridge, Massachusetts to southern Rhode Island (Fig. 1). The attitude of foliations developed in the shear zone varies along strike, from west dipping in the north, steepening through vertical southward, to north-east dipping in southern Rhode Island.

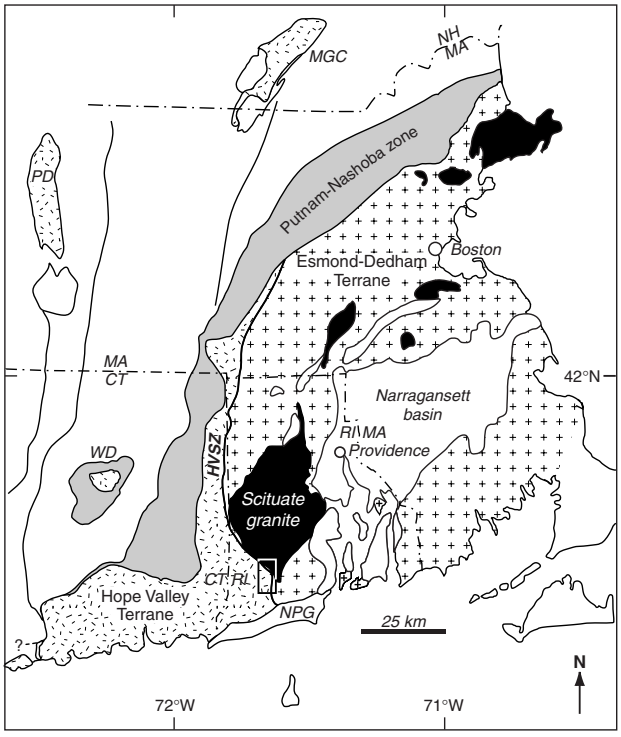

Fig. 1. Schematic geological map of south-eastern New England, with emphasis on the exposures of Avalonian crystalline rocks and some of the bounding structures. The Esmond–Dedham terrane and the Hope Valley terrane are major regions of Avalonian crystalline rocks, with additional exposures in structural culminations [Willimantic dome (WD), the Pelham dome (PD), and the Massabesic gneiss complex (MGC)]. Devonian Scituate granite and other Ordovician to Devonian alkalic granites shown in black. Note the truncation of the Scituate granite gneiss and other Esmond–Dedham rocks against the Hope Valley shear zone (HVSZ). NPG – Narragansett Pier granite. The box marks the area shown in Fig. 2. Geology drawn with modifications from Zen (1983), O'Hara & Gromet (1985), and Getty & Gromet (1988). From Gromet (1989).

A remarkable deformation gradient exists across the Esmond-Dedham terrane, from weakly and heterogeneously deformed rocks in north-eastern Rhode Island and adjacent Massachusetts, to increasingly penetratively deformed gneisses south-westward towards the Hope Valley shear zone. The gneisses are characteristically porphyroclastic and display a strong lineation and a weak to absent foliation. However, near Wyoming, Rhode Island, at the truncated south-western margin of the Esmond-Dedham terrane, the gneisses are non-porphyroclastic and mylonitic with a well-developed lineation and foliation. Deformation occurred at middle to upper amphibolite grade conditions and is inferred to record the late Palaeozoic juxtaposition of the Esmond-Dedham and Hope Valley terranes along a large-scale shear zone with a component of dextral displacement (O'Hara & Gromet, 1985; Getty & Gromet, 1988). U–Pb geochronology of metamorphically neocrystallized titanite from hornblende–biotite gneisses in the immediately adjacent Hope Valley terrane confirms that high grade deformation occurred at *c*. 292 Ma (Gromet, 1991).

An 800 m-long road-cut of Scituate granite gneiss was examined, which was located within one km of the contact with gneisses of the Hope Valley terrane (Fig. 2). The granite gneiss is very leucocratic and was originally mapped as the Late Proterozoic Hope Valley alaskite gneiss (Quinn, 1971), but subsequent geochronological studies indicate these rocks are Devonian Scituate granite (O'Hara & Gromet, 1985; Getty & Gromet, 1988).

FIELD OBSERVATIONS

Observations and measurements were made of lithological and structural features, including dominant mineralogy, texture, orientations of linear trends and foliation patterns, and the nature of pegmatite–gneiss relationships. Locations of samples taken for petrographic and isotopic study are shown in Fig. 2.

The road-cut consists of mylonitic Scituate granite and two distinct generations of pegmatite and related vein material. The mylonitic gneisses in this location are medium- to fine-grained with a strongly developed lineation and foliation. They are notably finer grained and much more strongly foliated than the vast majority of granite gneiss mapped as Scituate throughout central Rhode Island. Another important

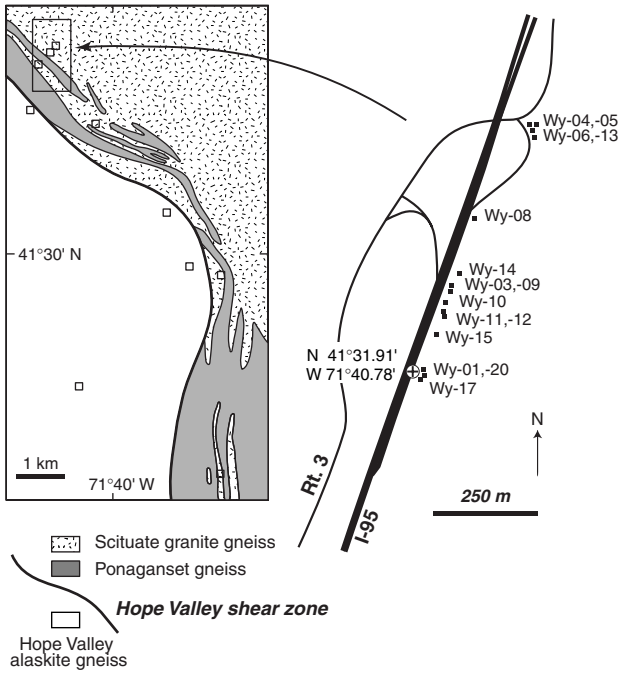

Fig. 2. Geological map of the Wyoming, RI area, from Getty & Gromet (1988). Open squares are geochonologically controlled sample locations from O'Hara & Gromet (1985) and Getty & Gromet (1988). Inset shows sample locations along road cut.

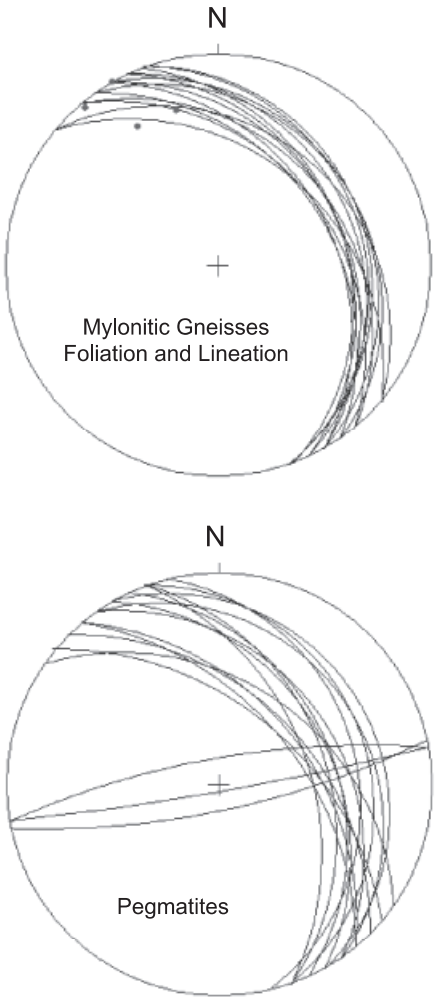

Fig. 3. Stereoplots (lower hemisphere) of foliation and lineation measurements and pegmatite orientations in the mylonitic Scituate granite gneiss along the road cut.

distinction is that the mylonitic gneisses at this road-cut lack porphyroclasts, whereas porphyroclasts of feldspar are extensively developed in the deformed Scituate granite gneisses elsewhere.

The major mineral assemblage of quartz + plagioclase + alkali feldspar + biotite ± hornblende remains in relatively uniform proportions over the area studied, with biotite and/or hornblende contents being more variable than others. There are minor zones of very leucocratic gneiss, typically containing $< 2\%$ dark minerals (e.g. Wy-01), in close proximity to gneisses with 5–8% dark minerals (e.g. Wy-20). These variations are inferred to reflect compositional variations inherited from the Devonian magmatic protolith.

Structures in Scituate granite gneiss

The mylonitic foliation generally strikes north-west and dips moderately to the north-east (Fig. 3), and is defined at the outcrop scale by aligned biotite and a fine compositional layering of quartz and feldspar aggregates. A sub-horizontal, north-west-trending mineral lineation (Fig. 3) is formed by an alignment of light and dark mineral aggregates (Fig. 4a). The lineation is difficult to identify in many exposures because of the massive and leucocratic character of the protolith, and the inability in many instances to view surfaces closely parallel to the lineation.

The orientation and penetrative nature of the foliation and lineation are generally consistently developed, but the grain size of the gneiss varies locally. At sample locality Wy-03, a strongly reduced grain size and an intense planar foliation characterize a narrow zone of ultramylonitic gneiss about 1 m thick (Fig. 4b). The foliation is defined by a very fine layering of quartz-feldspar and oxide aggregates, and is locally folded by small isoclinal recumbent folds (Fig. 4c). These appear to be synkinematic with the mylonitization.

The mylonitic gneisses locally contain both diffuse zones and layer-parallel lenses of variably foliated, leucocratic 'granite'. The diffuse zones are mostly unfoliated, forming irregularly shaped pockets or segregations of granite that fade into or replace the fabric of the host gneisses (Fig. 4d). Some of these pockets are associated with local deflections of the deformational fabric. The layer-parallel lenses of granite range from megascopically isotropic to somewhat more weakly foliated than adjacent gneisses. In many instances the lenses appear gradational into

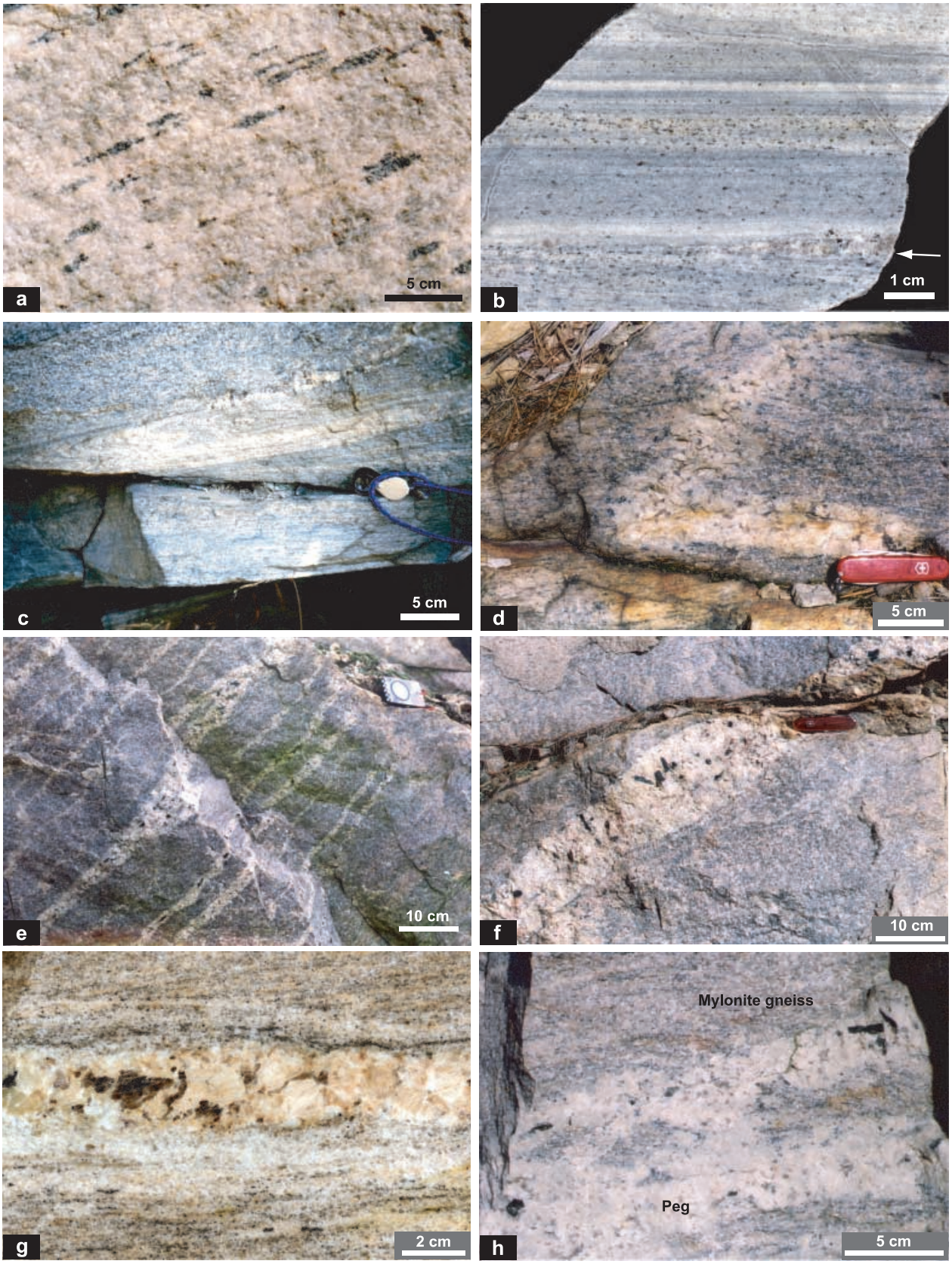

bounding mylonitic gneisses, whereas in others they are more distinct (e.g. a granitic wedge in ultramylonitic gneiss, Fig. 4b). The lenses are typically one to several cm thick (thinner in ultramylonitic gneiss) and generally extend several tens of cm parallel to foliation before fading into more typical mylonitic gneiss or wedging out. In some instances these lenses occupy locations adjacent to pegmatite or transitional between mylonitic gneiss and pegmatite, or are associated with rare inclusions of mylonitic gneiss found within pegmatite (see Fig. 4g,h). Thus these materials appear to be related to the syn- to late-tectonic pegmatites described below, but have less distinct walls and lack the coarse grain size of the pegmatites.

Pegmatites

The Scituate granite gneiss in this outcrop is host to two distinct generations of pegmatite. The most abundant set of pegmatites is syntectonic and has a mineral assemblage very similar to the Scituate granite: plagioclase + alkali feldspar + quartz ± hornblende. This similarity, and in particular the presence of hornblende as a magmatic phase in the pegmatite, indicates the pegmatites and their host Scituate granite gneisses are in substantial phase equilibration. Most pegmatites are between 2 cm and 1 m thick and are characteristically parallel or sub-parallel to the gneissic foliation (Fig. 3). One notable occurrence contains an array of a dozen thin pegmatite dykes, some coalescing (Fig. 4e). Pegmatites generally show no obvious internal strain in outcrop, and inequant minerals such as hornblende and feldspar generally display random orientations (Fig. 4f). However, many of the pegmatite dykes display slightly to moderately developed pinch-and-swell morphologies (i.e. boudinage) (e.g. Fig. 4f). The general structural concordance of this generation of pegmatites and their boudinaged yet undeformed interiors indicate a syntectonic to late tectonic emplacement. Smaller pegmatites commonly show a wispy, somewhat discontinuous biotite selvage along one or both walls (Fig. 4g), whereas others have an indistinct wall or walls and either fade into gneiss or grade into zones of mixed pegmatite-gneiss texture (e.g. Fig. 4h) or granitic texture (below pegmatite in Fig. 4g).

A second group of pegmatites is distinct in orientation and structure from the syntectonic generation. This group is characterized by the assemblage plagioclase + alkali feldspar + quartz, and is oriented approximately east–west with a sub-vertical dip (Fig. 3). These pegmatites cross-cut the tectonic foliation in the mylonitic gneisses and all other pegmatitic and quartz-rich vein material in the outcrop and do not show either boudinage or folding, and therefore record post-tectonic emplacement of pegmatite melt.

PETROGRAPHIC OBSERVATIONS

The rocks sampled for petrographic and microstructural study are classified into four groups for discussion: mylonitic gneiss, ultramylonitic gneiss, pegmatite and gneiss–pegmatite contact.

Mylonitic gneiss

Mylonitic gneiss is by far the most abundant lithic type, constituting more than 90% of this outcrop. In thin section, mylonitic gneisses have the mineral assemblage quartz + plagioclase microcline + biotite ± hornblende, with accessory titanite, zircon, chlorite and oxides. The maximum grain size of quartz and feldspar varies within and among samples, from 1.2 to 1.8 mm (Wy-09) to 1.6–4.0 mm (Wy-08). Most samples contain a population of finer quartz and feldspar grains ranging down to 200–400 μm.

Quartz occurs both as larger, generally irregular grains with complex phase boundaries, and as finer (< 500 μm) equant grains that have simple convex surfaces against surrounding minerals. The larger grains prominently display a chessboard extinction pattern (Fig. 5a), which is poorly developed or absent in finer grains. Microcline and plagioclase feldspars occur as distinct grains with well-developed gridiron and albite twinning, respectively. Feldspar lacks internal deformation (i.e. twins are commonly undeformed), and exsolution is rare. A small amount ($< 5\%$) of very fine exsolution lamellae is present in some large microcline grains in some samples (e.g. Wy-08), as is rare granular exsolution of plagioclase. Exsolution is not present in plagioclase. Hornblende and biotite contents are variable among the samples, ranging from <1 to 5%. Hornblende ranges up to 1.5 mm in diameter, is blue-green in colour, and shows a distinctively recessive, interstitial character to surrounding quartz and feldspar grains (Fig. 5b). Biotite grains are typically <1 mm in diameter and are

Fig. 4. Mylonitic gneisses, ultramylonitic gneisses, and pegmatites. (a) Hornblendic mylonitic gneiss showing typical strong lineation and foliation, viewed along a surface parallel to lineation; hornblende occurs as mixed-phase aggregates with quartz and feldspar (see Fig. 5b). (b) Ultramylonitic gneiss in sawn block, showing planar fabric defined by laminations of quartz-feldspar and oxide layers; small wedge of coarser grained granitic material is located in lower right, marked by arrow. (c) Folds in the ultramylonitic gneiss. (d) Pegmatite and gradational granite pocket, fading into and replacing mylonitic fabric (subhorizontal). (e) Part of an array of a dozen hornblendic pegmatite dykelets aligned with gneissic foliation; a few of the dykelets coalesce along strike. (f) A slightly boudinaged pegmatite; note large hornblende grains with random orientations. (g) Pegmatite and mylonitic gneiss in sawn block; note discontinuous biotite-rich selvage along the top of the K-feldspar-rich pegmatite dyke, the presence of a leucocratic, plagioclase-rich granitic lens immediately below the pegmatite, and the general structural concordance of the pegmatite with the mylonitic foliation; large dark grains in pegmatite are smoky quartz; sample Wy-01. (h) Example of coalescence of pegmatite dykes, with 'inclusions' of mylonitic gneiss; some leucocratic material bordering the inclusions is granitic textured.

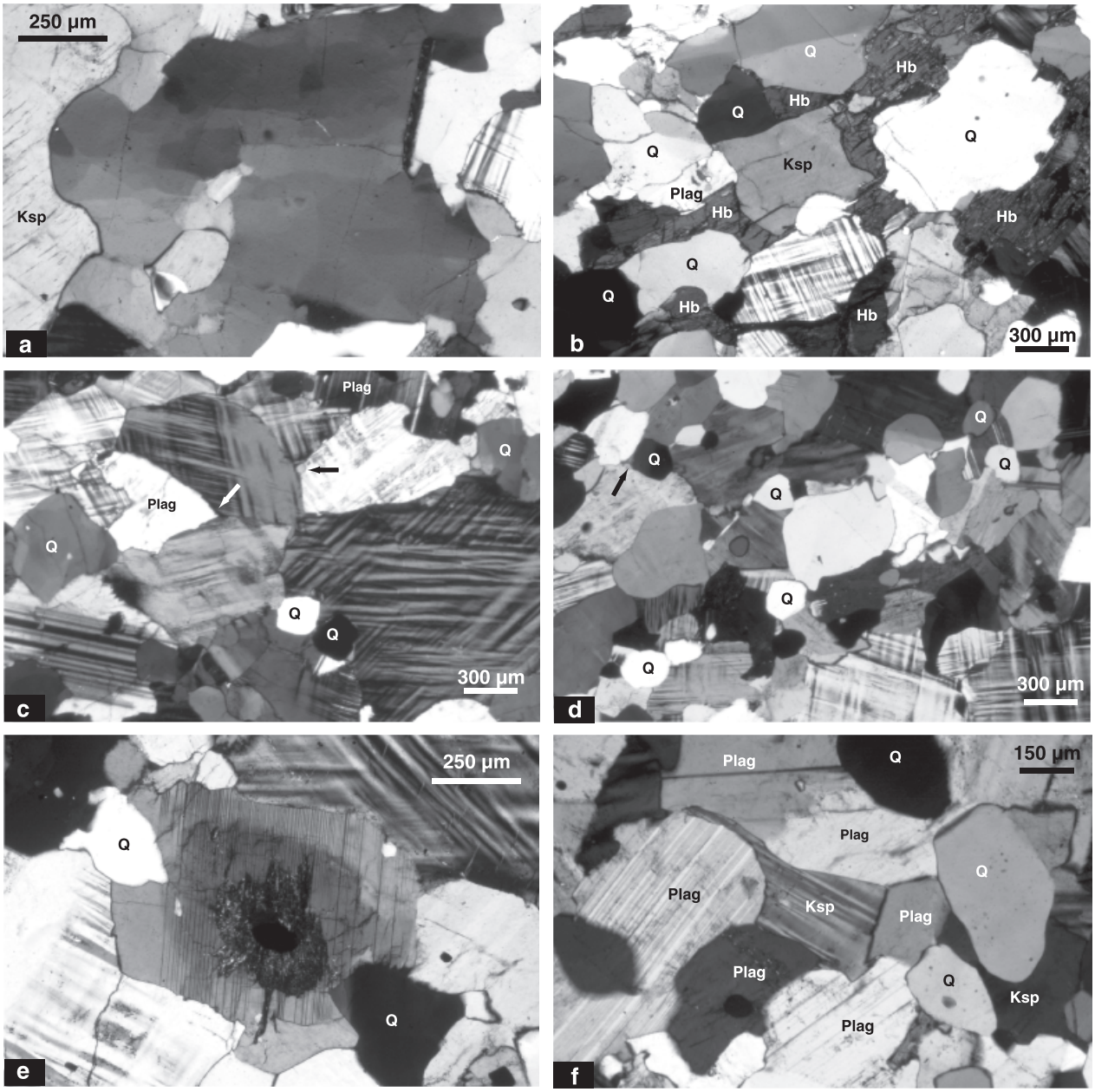

Fig. 5. Photomicrographs (crossed polarizers) illustrating heterogeneous mix of low-energy grain and high-energy phase boundaries in mylonitic gneisses. Abbreviations: Hb – hornblende; Plag – plagioclase; Ksp – K-feldspar; Q – quartz. (a) Chessboard extinction in large quartz grains in mylonitic gneiss; note lobate phase boundary between quartz and large microcline grain (labelled) on left side of image. (b) Interstitial nature of hornblende grains in hornblende-rich aggregates in lineated mylonitic gneiss (Fig. 4a); note that hornblende grains are dispersed about feldspar and quartz grains and appear to fill in potential spaces between them; some quartz grains exhibit phase boundary cusps; the six points labelled 'Hb' mark five different hornblende grains (with different extinctions), emphasizing that this image shows part of an aggregate of distinct hornblende grains, not one large poikiolitic hornblende grain. (c) Equilibrated grain boundaries among coarse microcline grains; note triple junctions among coarse microcline grains in the centre to upper left of the field of view; note plagioclase grain with phase boundary cusp against microcline grains (white arrow), and small equant quartz grains occupying boundaries (labelled quartz grains near centre) and intersections (black arrow) among microcline grains; labelled quartz grains show apparent indenting relationships to feldspar grains. (d) Many small equant quartz grains with apparent indenting relationships to neighbouring feldspar grains; arrow marks an example of an apparent interstitial relationship. (e) Equant quartz grains apparently indenting plagioclase and truncating compositional zoning. (f) Microcline grain with a 'pan handle' protrusion between two neighbouring plagioclase grains; note the smooth, 120° intersections of the same microcline grain with adjoining plagioclase grains; subequant quartz grains in the right half of the photo display apparent indenting relationships to neighbouring plagioclase and microcline grains.

generally recessive in nature. Small euhedral titanite crystals are spatially associated with grains of blue-green hornblende, all of which are aligned in the foliation.

The foliation is defined by a mineral shape fabric of biotite and hornblende, and layer-parallel concentrations of small oxide grains. Monophase aggregates of quartz and of feldspar help define the foliation in some samples, and many of the larger quartz and feldspar grains with aspect ratios of 2:1 or greater have a shape preferred orientation (e.g. Fig. 5b,d). The monophase aggregates presumably represent former coarse (>1 cm) igneous grains of feldspar and quartz, which are common throughout the less deformed interior of the Scituate granite pluton (Quinn, 1971; Day *et al.*, 1980).

The extent of microstructural equilibrium in these mylonitic gneisses is quite variable. In individual thin sections, equilibrated and non-equilibrated grain and phase boundary configurations are observed in close proximity. The well-equilibrated texture is characterized by predominantly straight to gently curved grain boundaries with approximately 120° intersections, such as microcline–microcline boundaries (Fig. 5c). Grain boundaries in microcline aggregates typically form a network of triple junctions, suggesting a high degree of textural equilibration. A remarkable feature of this texture is that it is well developed among the coarsest grains.

The non-equilibrated texture is characterized by irregular grain and phase boundaries showing interstitial, cuspate and lobate relationships. Quartz displays variable relationships, with significant differences correlating to grain size. Large quartz grains (>1 mm) have irregular, commonly ameboid shapes that interfinger to varying degrees with feldspars. Phase boundaries are lobate (Fig. 5a) and grain boundaries among the coarser grains are commonly lobate as well. Smaller quartz grains (< 500 μm) typically have rounded, equant shapes against feldspar. These smaller quartz grains appear to impose their equant shapes on neighbouring feldspar, causing cuspate outlines (Fig. 5c,d) and even overall interstitial relationships. In some instances, small equant quartz grains occupy triple junctions in microcline aggregates (e.g. at black arrow in Fig. 5c). Additionally, rare compositional zoning in plagioclase was observed to truncate against small equant quartz grains embedded in their rim (Fig. 5e).

These irregular phase boundaries appear to develop by the indentation of equant quartz into other phases. It is emphasized, however, that in most cases it can not be determined if such quartz grains indented pre-existing feldspar, implying a pressure solution or diffusion creep process, or if the feldspar grew to fill in space around quartz, which could result from metamorphic or igneous growth of feldspar. The significance of these relationships is discussed later.

Even where small equant quartz grains are absent, feldspar phase boundaries (i.e. microcline-plagioclase) are irregular. Narrow 'arms' of feldspar fill small spaces between larger grains of other feldspars, in some cases occupying the intersections of several larger grains (Fig. 5f). Quartz and feldspar grains also completely enclose the fine oxide grains distributed in thin folia parallel to the mylonitic fabric.

Ultramylonitic gneiss

The ultramylonitic gneisses have a mineral assemblage similar to that of the mylonitic gneisses: quartz + plagioclase + microcline + biotite, with accessory titanite, zircon, chlorite and oxides. Hornblende is absent, and biotite appears to be breaking down to fine-grained oxides and aggregates of euhedral titanite. Plagioclase and microcline occur as distinct grains and lack exsolution except in discontinuous zones of coarser feldspar and rare wedges of granite where some coarser (800 μm) microcline grains contain very fine exsolution lamellae. Chessboard extinction and other undulatory extinction are absent to weakly developed, respectively, among the quartz grains in the ultramylonitic matrix, but are well developed in the coarser, flattened quartz grains in the granitic wedges (Fig. 4b).

Ultramylonitic gneisses differ from mylonitic gneisses primarily by a smaller, more uniform grain size (typically 200–400 μm; Fig. 6a), a higher proportion of oxide, and a much stronger and more finely developed planar mineral layering, particularly that defined by fine grains of oxide (typically 20–70 μm). The oxide grains are concentrated into thin trains within the tectonic foliation. These trains define a more finely developed lamination than is present in the quartzofeldspathic matrix, yet individual oxide grains are commonly completely enclosed by recrystallized quartz and feldspar grains (Fig. 6b). These relationships suggest that the syntectonic grain sizes of quartz and feldspar were smaller than present grain sizes, and that grain and even phase boundaries were mobile (see later discussion). Microstructures of the ultramylonitic gneiss are similar in type to those of the mylonitic gneiss, but lower-energy grain and phase boundaries are more prevalent. Except for quartz in the granitic wedges, grains are equant to sub-equant and only a weak shape preferred orientation is apparent (Fig. 6a). These features and the more uniform grain size give the ultramylonitic gneiss a mosaic appearance in thin section (Fig. 6a).

Pegmatite

Pegmatite mineral assemblages are quartz + plagioclase + microcline ± hornblende with accessory biotite, chlorite and titanite. Textures in thin section are largely igneous, with unequilibrated, interdigitating grain and phase boundaries, as is commonly developed in multiply saturated magmas during cotectic crystallization. Large microcline grains contain as much as 20% exsolved plagioclase component, whereas

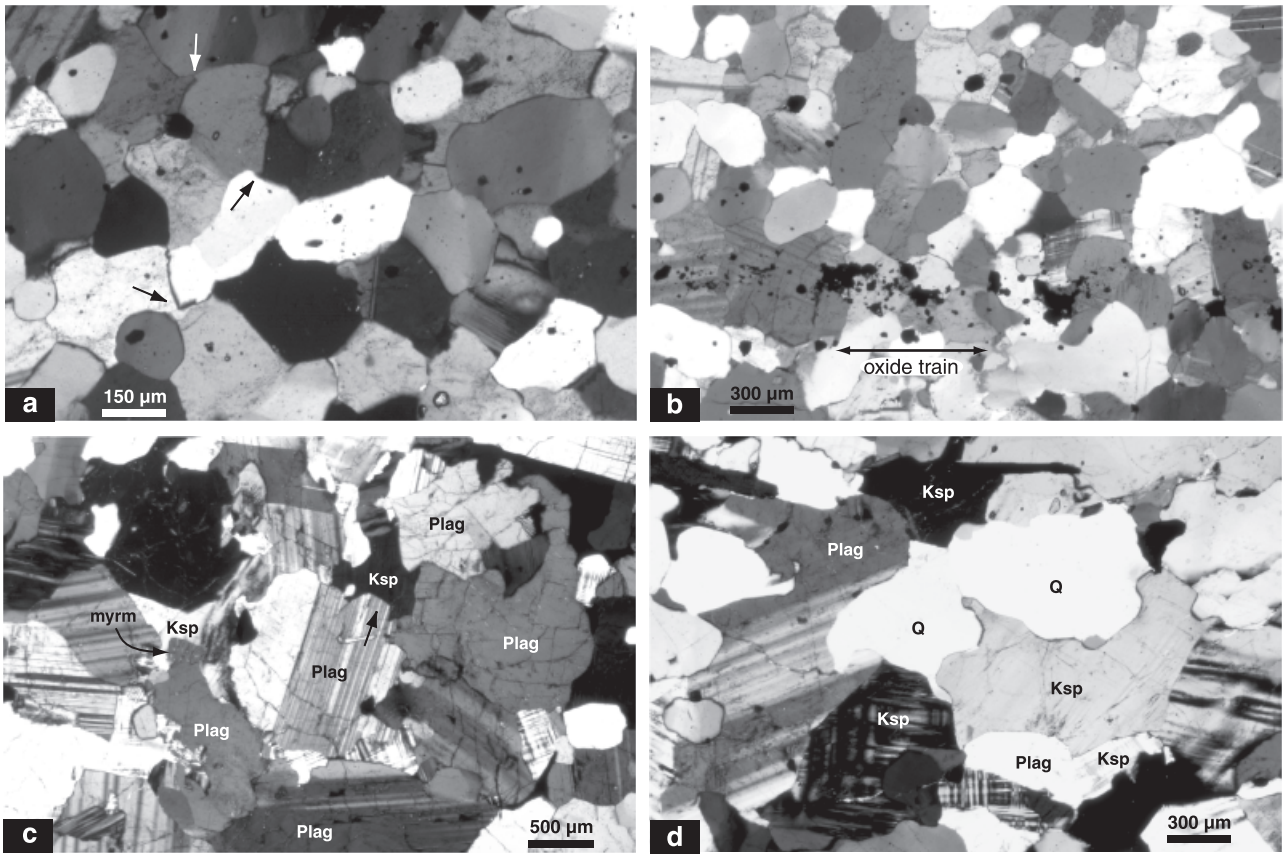

Fig. 6. Photomicrographs (crossed polarizers) illustrating microtextures of ultramylonitic gneisses and diffuse granitic lenses. Abbreviations as in Fig. 5 except as noted. (a) Mosaic texture typical of ultramylonitic gneiss; arrows indicate examples of fine-scale high-energy relationships, despite the overall equilibrated appearance. Note weak shape preferred orientation. (b) Example of quartz and feldspar enclosing oxide grains in a thin train paralleling the ultramylonitic foliation (horizontal in image); such engulfing relationships indicate a lack of pinning of quartz and feldspar grain boundaries; image taken with 'half crossed' polarizers to highlight oxide grain distribution. (c) Two smaller microcline grains (labelled grains near centre and centre-left) displaying interstitial relationships among several adjoining plagioclase grains, suggesting the microcline grains mimic the location of former melt pools; straight arrow marks one example of a plagioclase lath with apparent rational faces against the microcline in one of these apparent melt pools; the top of the left-most labelled plagioclase grain extends into the other apparent melt pool and develops rare myrmekite (myrm) along part of their boundary; from diffuse granitic lens adjoining pegmatite in Wy-01 (see Fig. 4g). (d) Example of mutually interstitial relationships among quartz and feldspar grains in diffuse granitic lens (also Wy-01); note the small arm of quartz extending between two labelled microcline grains near centre-left of figure, but also the tendency of the two labelled quartz grains to develop rational faces against the large labelled microcline grain near centre-right of figure.

plagioclase shows only minor exsolution; granular exsolution of plagioclase from microcline is locally but sparingly developed. In Wy-11, biotite rims a hornblende grain in apparent reaction relationship. Evidence of minor solid state deformation in the early, boudinaged pegmatites includes kink bands off-setting albite twins, zones of tapered albite twins, and large quartz grains with chessboard extinction. These features confirm the syntectonic emplacement of the first generation of pegmatites.

Gneiss–pegmatite contact

The contacts between pegmatite and gneiss are marked by a transition in grain size from 2 to 20 mm quartz and feldspar in pegmatite, to the < 2 mm grains in the mylonitic gneiss. This transition is commonly abrupt, but diffuse leucocratic granitic-textured lenses are found along segments of some gneiss–pegmatite contacts (Fig. 4g). Where examined petrographically (Wy-01), such lenses are plagioclase-rich with some quartz and interstitial microcline (Fig. 6c). These lenses thus appear to be compositionally complementary to the adjacent microcline-rich, plagioclase- and quartz-poor pegmatite (i.e. together constitute a granite-minimum composition). In some cases, the plagioclase or quartz of these lenses occur as discontinuous monophase zones of intermediate grain size locally separating the pegmatite from the finer-grained minerals in the mylonitic gneiss, indicating a degree of petrographic continuity between pegmatite, granitic lenses and gneiss (cf. Marchildon & Brown, 2003). The

microstructures of the granitic lenses have several similarities to those of the mylonitic gneisses: an abundance of high-energy phase boundaries among quartz and feldspar, chessboard extinction in quartz, and a lack of exsolution in microcline and plagioclase feldspar. However, the microstructures in these lenses differ in that the quartz and feldspar all behave similarly, showing mutual interstitial relationships among themselves in varying instances (Fig. 6d), and there is a tendency for plagioclase and quartz to develop rational faces against some microcline grains (Fig. 6c,d). Some microcline grains display interstitial relationships to other minerals extending over several neighbour grains, and a few instances of myrmekitic intergrowths in plagioclase occur along part of its boundary with interstitial microcline (Fig. 6c). Myrmekite is absent from the mylonitic gneisses. Some plagioclase grains exhibit core-rim zoning.

The significance of the microstructures in the granitic lenses is unclear. The mutual interstitial relationships, interstitial microcline forming apparent pools between neighbouring grains (cf. Sawyer, 2001), and the localized myrmekite development against such pools correspond to what is expected of crystallization from melt. The mutual interstitial relationships are consistent with cotectic crystallization, where apparent conflicts in the order of crystallization and variably subhedral to anhedral grains develop locally due to the vagaries of grain impingement during simultaneous growth from melt (e.g. Flood & Vernon, 1988; Vernon & Collins, 1988). Myrmekite is known to develop either by igneous or metamorphic replacement (e.g. Hibbard, 1979 and Simpson & Wintsch, 1989, respectively). In the latter case, myrmekite characteristically develops as protuberances into existing K-rich feldspar and shows a specific geometrical relationship to the deformational fabric. These features are lacking in the present case, and myrmekite is only observed in these granitic-textured zones, not at any of the plagioclase–microcline boundaries in the mylonitic gneisses. Thus several microstructural features suggest the granitic lenses are igneous in origin, and could represent the first phases to crystallize from the pegmatite, or crystallization of melt drawn into small dilatant zones that developed at pegmatite-gneiss contacts as they were being deformed.

U–Pb AND Rb–Sr ISOTOPIC RESULTS

U–Pb zircon and titanite ages

Zircon and titanite were separated from a typical example of the mylonitic gneiss (Wy-17) to determine the magmatic age of the granite protolith and the age of its deformation/metamorphism, respectively (Tables 1 & 2). Four fractions consisting of several clear prismatic zircon each yielded markedly discordant U–Pb ages of 350–335 Ma (Fig. 7a). The results form an imperfect array with a limited spread that intersects concordia very obliquely. Consequently, the intercepts at *c*. 385 Ma and 240 Ma both have large uncertainties. These data do not provide a precise age for the magmatic crystallization of the granite protolith, but they confirm the earlier assignment of these rocks to Devonian Scituate granite gneiss on the basis of Rb–Sr whole-rock isochron results (O'Hara & Gromet, 1985; Getty & Gromet, 1988). The *c*. 385 Ma age is also consistent with the less discordant zircon U–Pb ages of *c*. 370 Ma reported for weakly deformed Scituate granite in central Rhode Island (Hermes & Zartman, 1985).

Four fractions of clear, subhedral to euhedral titanite grains were selected for U–Pb analysis. Such grains form part of the neocrystallized metamorphic mineral assemblage and are expected to record the age of titanite growth during the deformational/metamorphic event. The titanite have relatively low U/Pb ratios and therefore experienced very little growth of ^{207}Pb, precluding a concordia treatment. The U–Pb

Table 1. Wy-17 Zircon U/Pb data.

Sample	wt. (mg)	U p.p.m.	Pb p.p.m.	^{206}Pb/^{204}Pb measured	^{206}Pb/^{238}U (± err, abs)	^{207}Pb/^{235}U (± err, abs)	^{206}Pb/^{238}U Age, Ma	^{207}Pb/^{235}U Age, Ma	^{207}Pb/^{206}Pb Age, Ma
Zrn 1	0.03	529.9	28.75	1457.5	0.05392 ± 13	0.4005 ± 15	338.6 ± 0.8	342.0 ± 1.3	365.7 ± 6
Zrn 2	0.03	315.7	17.18	599.9	0.05401 ± 13	0.3976 ± 17	339.1 ± 0.8	339.9 ± 1.4	345.4 ± 8
Zrn 3	0.02	405.3	22.31	2357.5	0.05506 ± 16	0.4071 ± 19	345.5 ± 1	346.8 ± 1.6	355.2 ± 8
Zrn 4	0.02	585.2	30.99	3153.6	0.05310 ± 13	0.3911 ± 14	333.5 ± 0.8	335.2 ± 1.2	346.9 ± 6

(a) weights are visually estimated and subject to large uncertainties, and therefore U and Pb concentrations also have large absolute uncertainties.
(b) Pb ratios except measured ^{206} Pb/^{204}Pb are corrected for a blank of 5 ± 2.5 pg and mass fractionation of 0.08 ± 0.03%/amu.

	Description
Zrn 1	6 grains, irregular, clear to slightly cloudy
Zrn 2	4 grains, 2:1 prisms, clear
Zrn 3	5 grains, 2:1 prisms, clear, abraded
Zrn 4	5 grains, 2:1 prisms, clear, abraded

Table 2. Wy-17 Titanite U/Pb data.

Sample	$^{238}U/^{204}Pb$	err percentage	$^{206}Pb/^{204}Pb$	err percentage	err correlation
Ttn 2	961.58	1.4	60.762	0.972	0.928
Ttn 3	752.84	2.02	51.974	1.22	0.936
Ttn 4	913.72	1.61	60.028	1.11	0.933
Ttn 5	800.08	0.988	53.504	0.593	0.895
Fsp 1	0.0798	4.06	18.667	0.0671	0.0165

	Description
Ttn 1	2 grains, large, brown, cracks, inclusions, translucent
Ttn 2	18 grains, 12 med 5 fine + fragments, clear, few inclusions, faceted
Ttn 3	12 grains, 11 med 1 fine, clear, few or no cracks, faceted
Ttn 4	16 grains, 12 med 4 fine + fragments, clear, few or no cracks, faceted
Ttn 5	17 grains, 15 med 2 fine, clear, few or no cracks, faceted
Fsp 1	cloudy, cleavage

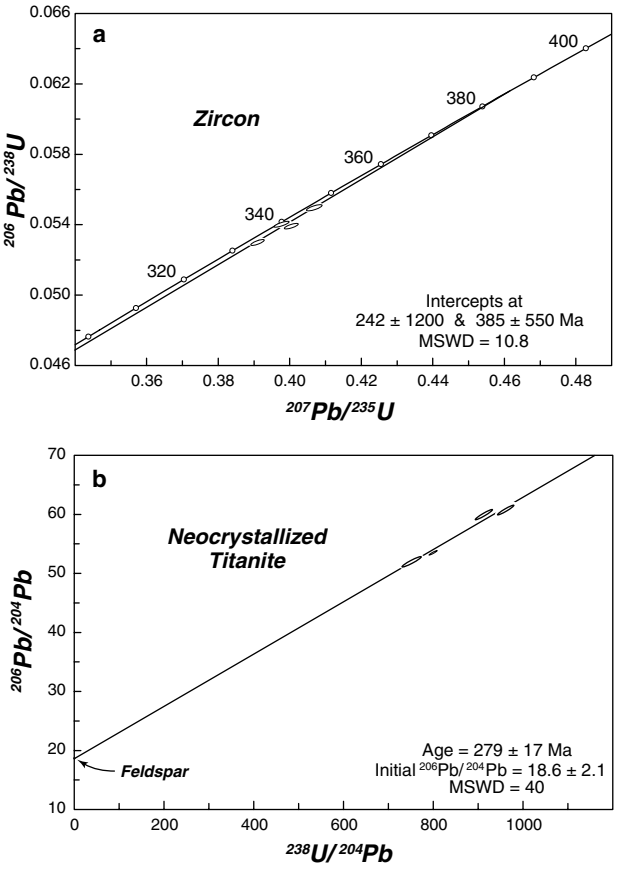

Fig. 7. U/Pb isotopic results from mylonitic gneiss Wy-17. (a) U-Pb concordia diagram for zircon. (b) ^{238}U-^{204}Pb isochron results for neocrystallized titanite and feldspar.

results are shown on a ^{238}U–^{206}Pb isochron diagram (Fig. 7b), where titanite and coexisting metamorphic feldspar form an imperfect isochron (scatter beyond analytical errors) with an age of 279 ± 17 Ma. These results indicate that the Devonian granite protolith was subjected to deformation and associated metamorphic neocrystallization of titanite during the Alleghanian orogeny. The lack of complete isotopic equilibration among the fractions is significant, and is discussed further in a later section.

Rb–Sr isotopic results

The Rb–Sr systematics of two different samples of pegmatite and their immediate wall rocks (Wy-01 and Wy-20c) were determined to evaluate the possibility that the pegmatites were derived by partial melting of local wall rock gneisses. Both samples contain syn- to late-tectonic (i.e. slightly boudinaged) pegmatite layers 1–3 cm thick hosted in mylonitic gneiss, forming part of the dyke array shown in Fig. 4(e). Even though the sample sites are separated in the field by only 2 m, their mineralogy differs. The pegmatite and wall rock of Wy-01 lack hornblende, and the pegmatite feldspar is predominantly potassic feldspar. In contrast, the pegmatites and wall rock of Wy-20c contain hornblende, and the pegmatite feldspar is predominantly plagioclase.

A sawn slab of each sample was sub-sampled to provide material from the pegmatite and surrounding wall rock gneisses (Fig. 8). The sub-samples consist primarily of single feldspar grain fragments from pegmatite and wall rocks, but sub-samples from Wy-01 also include two 'whole rock' materials prepared by powdering small approximately 2 g pieces of wall rock gneiss. Sub-samples were taken along a transect approximately normal to the pegmatite layers, with the most distant materials in each sample being separated by about 10 cm (Fig. 8).

The results for both sample locations (Table 3) are shown together on a Rb–Sr isochron diagram (Fig. 9). Pegmatite feldspar are plotted as filled symbols to differentiate them from wall rock materials. The sub-sample results for each sample show large scatter, indicating that the pegmatite and the immediate wall rock materials in each case did not come into Sr isotopic equilibration, despite their close spatial association. The extent of scatter is extreme for sample Wy-01 and precludes a meaningful age calculation. For Wy-20c the scatter also far exceeds analytical error (mswd = 42 482), but the results form an approximate linear array, yielding an errorchron of 274 ± 13 Ma. This age overlaps the 279 ± 17 Ma ^{238}U-^{206}Pb isochron age for neocrystallized titanite in Wy-17 (located just a few metres south of these samples) and the known ages of 295–275 Ma for Alleghanian metamorphism and igneous activity in the area (e.g. Hermes & Zartman, 1985; Gromet, 1991; Gromet *et al.*, 1998).

The most surprising results are that, despite the scatter, the two closely spaced pegmatite-wall rock systems have very distinct Rb–Sr isotopic systematics, and that the pegmatite materials in each case are clearly grouped with their immediate wall rocks. The details and significance of these observations are addressed below.

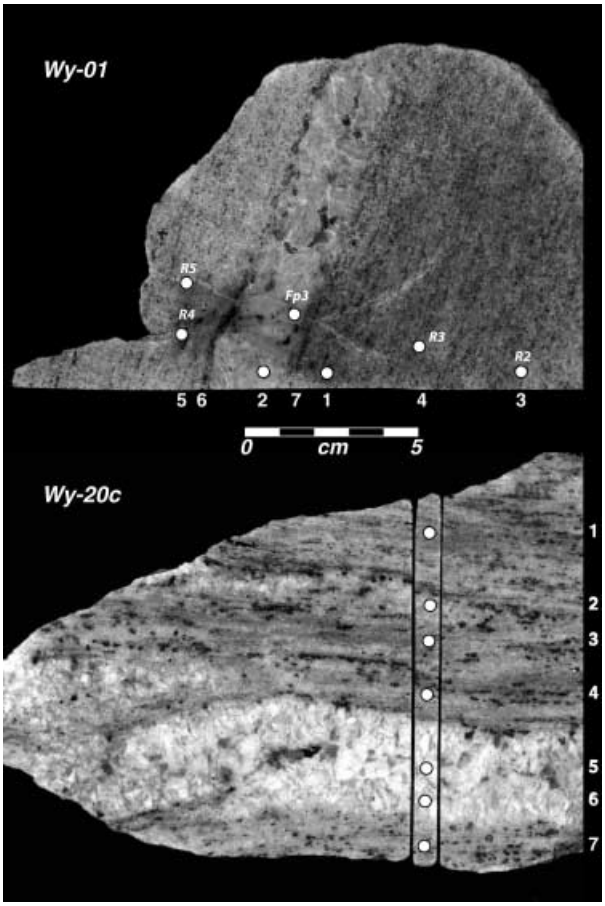

Fig. 8. Sub-samplings of pegmatite-gneiss samples Wy-01 and Wy-20c (sawn blocks). Numbers on margins refer to marked locations immediately above (Wy-01) or to the left (Wy-20c), and correspond to analyses in Table 3. Gneiss and pegmatite in Wy-01 lack hornblende (dark grains are smoky quartz), whereas those in Wy-20c contain hornblende. Note presence of two pegmatite layers in Wy-20c, a thicker one along the lower section and a thinner one above; both were sampled. Upper pegmatite has somewhat diffuse boundaries, and lower pegmatite is composite, with an intervening septum of gneiss and somewhat diffuse boundaries in the left part of figure.

Table 3. Rb–Sr analytical results.

Sample	wt (mg)	Rb_{ppm}[a]	Sr_{ppm}[a]	$^{87}Rb/^{86}Sr$[b]	$^{87}Sr/^{86}Sr \pm 2s_m$[c]	$^{87}Sr/^{86}Sr_I$[d]
Wy-01 mylonite gneiss-pegmatite (kspar-rich)						
1 gneiss	3.85	173.7	32.07	16.19	0.795311 ± 40	0.73219
2 pegmatite feldspar	1.18	314.9	32.11	28.79	0.856792 ± 33	0.74454
3 gneiss	11.82	178.0	26.46	19.18	0.813436 ± 19	0.73865
4 gneiss feldspar	3.01	132.3	17.73	21.86	0.838654 ± 11	0.75341
5 gneiss feldspar	1.66	123.6	23.74	15.22	0.811621 ± 12	0.75228
6 gneiss feldspar	1.45	408.2	44.45	26.90	0.834068 ± 11	0.72921
7 pegmatite feldspar	1.10	131.6	30.48	12.61	0.799636 ± 17	0.75049
Wy-20c mylonite gneiss-pegmatite (plagioclase-rich)						
1 gneiss feldspar	5.16	281.4	53.28	15.390	0.778942 ± 12	0.71894
2 pegmatite feldspar	2.00	439.7	80.54	15.903	0.778010 ± 13	0.71602
3 gneiss feldspar	1.19	461.1	81.46	16.496	0.781258 ± 16	0.71695
4 gneiss feldspar	0.59	227.4	88.42	7.471	0.747377 ± 21	0.71825
5 pegmatite plag.	3.85	1.84	120.0	0.044	0.716004 ± 8	0.71584
6 pegmatite plag.	5.60	4.36	123.2	0.102	0.717919 ± 8	0.71752
7 gneiss feldspar	2.36	35.85	90.26	1.151	0.722928 ± 9	0.71844

[a] Laboratory blanks for Rb and Sr are <0.4 ng.
[b] Error in $^{87}Rb/^{86}Sr$ is $<0.2\%$.
[c] $^{87}Sr/^{86}Sr$ corrected for natural Rb with $^{87}Rb/^{86}Sr = 0.38571$. $2\sigma_m$ errors are absolute. Analyses of NBS 987 Sr standard in period of analyses ranged from 0.710142 ± 7 to 0.710133 ± 9.
[d] Initial $^{87}Sr/^{86}Sr$ calculated to 274 Ma.

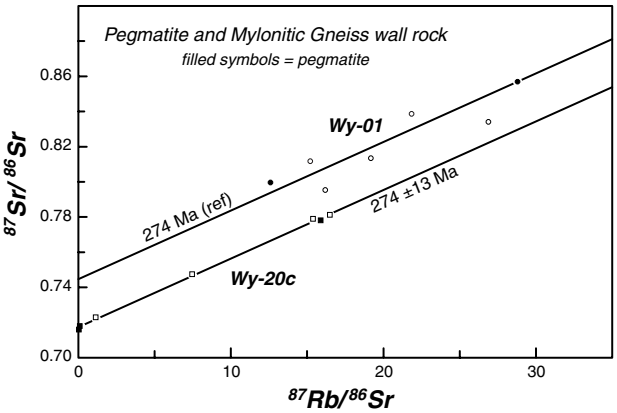

Fig. 9. Rb–Sr isochron diagram for sub-samples of pegmatite-gneiss samples Wy-01 (circles) and Wy-20c (squares). Filled symbols denote pegmatite. Both samples show excessive scatter. Data point symbols far exceed the size of analytical errors (symbols scaled to error would not be visible in this plot). The 274 ± 13 Ma errorchron for Wy-20c was determined by a Model 3 regression (Ludwig, 2001), and is associated with very large scatter (mswd = 42 482). Even more extreme scatter in Wy-01 precludes a meaningful age calculation; the 274 Ma (ref.) line is shown for comparison purposes only, but is believed to represent the igneous age of the pegmatite. Note the isotopic distinction between the two sample sets, yet the close association of the pegmatites with their immediate host gneiss in each case.

DISCUSSION AND INTERPRETATIONS

The primary motivation for this study was to identify the deformation mechanisms responsible for the development of a thick zone of mylonitic to ultramylonitic gneisses at high regional metamorphic temperatures. The microstructural observations reported above provide insights into the specific deformation processes involved and the conditions under which they occurred. The field relationships, mineral assemblages, and Rb–Sr isotopic properties of the mylonitic gneisses and associated syntectonic pegmatites provide evidence for the development of syntectonic partial melts in these gneisses, which in turn provides important context for interpretation of the deformation mechanisms involved.

The most significant result of the petrographic observations is that microstructures in the mylonitic and ultramylonitic gneisses are heterogeneous on the thin section scale, displaying an intimate mix of high-energy phase boundaries (ranging from cuspate/lobate to interstitial) and low-energy grain boundaries. The prevalence of both high-energy phase boundary configurations and low-energy grain boundary configurations presents a fundamental problem in the interpretation of deformation conditions and mechanisms for these rocks. As discussed below, this combination of microstructures could not have been

formed by dislocation creep or static recrystallization alone. Other processes must have contributed. The possibilities include diffusion creep and partial melting, either alone or in combination, both of which are of particular interest as they could strongly influence the rheology of the gneisses.

The discussion below seeks to develop constraints on whether deformation at the south-western margin of the Esmond–Dedham terrane developed in a localized weak zone resulting from a switch in the dominant deformation mechanism from dislocation creep to diffusion creep and/or the presence of local partial melts. This issue is of considerable significance to the evolution of the Hope Valley shear zone, as well as the understanding of the rheological behaviour of crustal rocks in orogens.

Field, petrographic and Rb–Sr isotopic evidence for syntectonic melts

There are several field and petrographic observations that provide evidence that the Scituate mylonitic gneisses developed syntectonic partial melts. First, syntectonic pegmatites and less distinct granitic lenses are distributed through the mylonitic gneisses. The lenses appear to represent partial melts that did not manage to segregate into distinct layers as the pegmatite magmas did, or possibly back-reacted with the gneiss. A genetic relationship between some pegmatite dykes and adjacent granitic lenses is suggested in cases such as sample Wy-01 (Fig. 4g), where an unusually microcline-rich pegmatite and adjacent plagioclase-rich granitic lens appear to be complementary (i.e. together constitute a granite minimum composition). As discussed earlier, this plagioclase-rich granitic lens displays petrographic features suggestive of interstitial melt (Fig. 6c). Note that because the host Scituate granite gneisses have compositions close to the granite minimum, little compositional contrast is expected between local partial melts and host gneisses.

Second, some of the syntectonic pegmatites occur as relatively thin, layer-parallel to layer-subparallel dyke arrays (Fig. 4e), whose form is analogous to melt segregation bands formed in melt-present deformation experiments (Holtzman *et al.*, 2003) and to foliation-parallel leucosomes observed in some migmatites, such as anatectic gneisses marginal to the South American shear zone in Brittany (Marchildon & Brown, 2003). These features suggest that the pegmatitic dykes are syntectonic accumulation channels for locally derived melts rather than distribution channels for externally generated melts injected into the gneisses, an inference that is strongly confirmed by the isotopic data (see discussion below). Moreover, the noted similarity of mineral assemblages among the syntectonic pegmatites (and the granitic lenses) and the immediately adjacent mylonitic gneisses implies a close genetic relationship between the syntectonic pegmatites and their host gneisses. Such evidence for chemical and isotopic equilibration or buffering between the pegmatites and the host gneisses is most easily explained by local melt contributions from the gneisses.

Third, the chessboard pattern of extinction in quartz (Fig. 5a) is known to form only at high temperatures (>650 °C; Mainprice *et al.* 1986), which equal or surpass the solidus of the Scituate granite in the 'wet' conditions indicated by the presence of biotite and hornblende and of pegmatites. The chessboard pattern in quartz arises from sub-grain boundaries developed under a combination of active prism [c] and basal <a> slip (Kruhl, 1996). Prism [c] slip is active only at very high temperatures, and can be recognized by a strong concentration of c-axes parallel to the inferred shearing direction (Mainprice *et al.*, 1986). Crystallographic preferred orientations of quartz c-axes parallel to the stretching lineation in other gneisses along the Hope Valley shear zone (O'Hara & Gromet, 1985) also imply high temperature deformation (>650 °C) over a broader area in this region.

Given these field and petrographic observations suggesting the presence of partial melts during deformation, and the importance of intergranular melt in influencing deformation mechanisms, we sought to more definitively determine if the Scituate granite gneisses were subjected to *in situ* partial melting during deformation. This possibility can be evaluated quite sensitively through the Rb–Sr isotopic systematics of the pegmatites and their immediate wall rocks due to the highly evolved and partly alkalic nature (Hermes & Zartman, 1985) and high Rb/Sr ratios (O'Hara & Gromet, 1985) of the Devonian Scituate granite, which results in a highly radiogenic protolith for mylonitic gneisses by *c.* 275 Ma.

Both the wall rock gneisses and the pegmatites are indeed highly radiogenic, yielding present-day $^{87}Sr/^{86}Sr$ ratios between 0.7160 and 0.7813 for Wy-20c and between 0.7953 and 0.8568 for Wy-01. The pronounced scatter in the Rb–Sr isotopic results (Fig. 9) shows that, in each case, isotopic equilibration was not achieved between pegmatite and wall rock, even though sub-samples in each case are separated by only several centimetres or less (Fig. 8). The scatter could be considered as evidence that the pegmatites were not derived from the wall rocks as partial melts, based on the expectation that a mobile interstitial melt would be effective in promoting isotopic equilibration over these length scales. However, a more complete consideration of the distinctions between the two pegmatite-wall rock samples leads to a different conclusion.

The key observation is that despite the lack of very local equilibration, the two groups of sub-samples of wall rock gneisses are quite distinct on a Rb–Sr isochron diagram (Fig. 9), forming parallel arrays with a similar *c.* 275 Ma slope but very different initial ratios. This indicates that these closely spaced sample sets, separated by only 2 m in the field, represent distinct Rb–Sr isotopic systems that remained

chemically isolated from each other through the Alleghanian deformation and metamorphism. Most remarkably, the pegmatites in each case are closely grouped with their immediate wall rocks (Fig. 9). The isotopic similarity among each pegmatite and its adjacent wall rocks, but the isotopic contrast between the two pegmatite-wall rock systems, constitute strong evidence that the pegmatites are genetically related to their immediate wall rocks. Analogous correspondences with the same implications exist in the mineralogy of the pegmatites and wall rocks: those from sample Wy-20c both contain hornblende, whereas those from sample Wy-01 both lack hornblende.

These results demonstrate conclusively that the mineralogical and isotopic compositions of the pegmatites are controlled by the mineralogy and isotopic composition of their immediate wall rocks, not by a common magma generated externally to the outcrop area. Because the wall rock gneisses were unable to reach complete Sr isotopic equilibration at this time, it is not surprising that the melts that formed from them show local heterogeneity. It is notable in this regard that the age-corrected $^{87}Sr/^{86}Sr$ ratios of each of the pegmatites (see Table 3) fall near an approximate average of those of the immediately surrounding wall rock gneisses. Thus the ratios appear to correspond to a rough mix of material derived from the immediately adjacent wall rocks.

The most important factor in creating the marked Sr isotopic heterogeneity observed within the wall rock gneisses is the very high and variable Rb/Sr ratios in the Devonian Scituate granite protolith (O'Hara & Gromet, 1985; Getty & Gromet, 1988). In the approximately 100 Myr between the emplacement of the Scituate granite at *c*. 370 Ma and the Alleghanian orogenic event at *c*. 275 Ma, the high and variable Rb/Sr ratios produced very radiogenic and highly variable $^{87}Sr/^{86}Sr$ ratios in the gneisses.

The above features argue that the pegmatite magma formed by local partial melting of isotopically and mineralogically heterogeneous wall rock gneisses. Because field relationships clearly indicate the pegmatites are syntectonic, we conclude that deformation in the gneisses occurred in the presence of intergranular melts. It remains surprising that neither penetrative deformation nor partial melting and extraction of local partial melts over short distances to form the pegmatites was sufficient to erase the isotopic heterogeneity. The preservation of isotopic heterogeneity over such small length scales in wall rock gneisses also appears to be reflected in the scatter in the $^{238}U/^{206}Pb$ isochron results for titanite from Wy-17 (Fig. 7b). A key factor in both cases may be that deformation by diffusion creep and grain boundary sliding (see discussion below) does not repeatedly cycle grain interiors to grain boundary locations, as happens when dislocation creep is accommodated by grain boundary migration recrystallization, and thus isotopic equilibration among nearby grains is limited by slow volume diffusion (see discussion in Gromet, 1991).

Microstructural evidence for dynamic recrystallization, static recrystallization and melt-enhanced diffusion creep

Dynamic recrystallization

Microstructural evidence for dynamic recrystallization accompanying dislocation creep in the mylonitic gneisses is strong, but primarily limited to coarser grains, particularly quartz. Wavy grain boundaries are commonly developed between coarser quartz grains, and are indicative of grain boundary migration recrystallization (regime 3 of Hirth & Tullis, 1992). Chessboard extinction in coarser quartz is indicative of high-temperature sub-grain formation (Kruhl, 1996). The microstructural features of equant to sub-equant grains with low internal strain and a weak shape preferred orientation, as observed in the finer-grained domains of the mylonitic and ultramylonitic gneisses, also could have arisen from dynamic recrystallization by grain boundary migration (e.g. Hirth & Tullis, 1992; Stipp *et al*., 2002; Tullis, 2002), but these features could also be produced by competing processes for which additional evidence exists (see discussion below). Other features indicative of dynamic recrystallization accompanying dislocation creep, such as mantled porphyroclasts of feldspar, are notably lacking. It is possible, however, that the monophase aggregates of microcline were subject to dynamic recrystallization by grain boundary migration earlier in the deformation history, but their internal grain boundaries appear to have been modified by late- to post-tectonic static recrystallization (see discussion below).

Whereas dynamic recrystallization accompanying dislocation creep is capable of producing microstructures with straight, curved or lobate grain boundaries, this process does not directly modify phase boundaries (e.g. quartz-feldspar). Therefore the abundance of high-energy phase boundaries observed in the Scituate mylonitic gneisses cannot be explained by dynamic recrystallization accompanying dislocation creep.

Static recrystallization

A low energy grain boundary microstructure can be produced by static recrystallization, a high-temperature process that allows minimization of surface and internal energy through grain coarsening and textural equilibration (Vernon, 1968). Static recrystallization will also allow phase boundaries to equilibrate by adjusting their shapes and interfacial angles (e.g. Vernon, 1968, 1976), but grain growth will be limited by compositional pinning. In the mylonitic gneisses, the straight to gently curved grain boundaries and network of triple junctions in coarse-grained microcline aggregates (e.g. Fig. 5c) strongly suggests that these grains achieved their present size and grain

boundary microstructure by static recrystallization. Instances of locally irregular grain boundaries exist, but most of these are observed to be pinned by small impurities and the few remaining ones are attributable to a small increment of late strain. The syn-deformational grain size in the mylonitic gneisses is estimated to have been no more than 500 μm, the size of the largest grains that do not show evidence of having been coarsened by static recrystallization.

Another feature suggestive of an approach to textural equilibration in the mylonitic gneisses is the presence of small equant quartz grains at triple junctions of coarse microcline grains in monophase aggregates (Fig. 5c). Due to the fact that like–like (i.e. grain) boundaries commonly have higher energy than unlike (i.e. phase) boundaries, the interfacial energy in a rock with monophase aggregates will be reduced by nucleating and growing unlike phases at high-energy sites at triple grain junctions and grain boundaries (Vernon, 1976; Dallain *et al*., 1999). We suggest that this is the most attractive explanation for the occurrence of quartz grains in the interiors of what were originally large potassium feldspar grains.

Static recrystallization is also evident in the ultramylonitic gneisses, where most grains are equant or sub-equant, there is little internal lattice deformation, and most grain and some phase boundaries are smooth and straight or gently curved (Fig. 6a). Particularly significant are the observations that trains of small oxide grains form finely laminated folia parallel to the strong planar foliation, and quartz and feldspars commonly have overgrown and engulfed the oxide grains within the folia (Fig. 6b). The fine folia of oxide grains define planes that do not deflect around quartz and feldspar grains, indicating that the thin folia had to have been shaped by the mylonitic deformation when the grain sizes of the adjoining matrix grains (quartz and feldspars) were much finer than they are presently. These features suggest that following an earlier period of grain size reduction during mylonitization, late- or post-deformational grain growth occurred in the matrix grains, overgrowing small impurities such as the oxides. However, the persistence of a much finer grain size in the ultramylonitic gneisses compared to the mylonitic gneisses still requires explanation.

Petrographic examination confirms that most grains in the mosaic matrix of the ultramylonitic gneisses (Fig. 6a) have phase boundaries rather than grain boundaries, and therefore are compositionally pinned. A weak shape preferred orientation is evident in the matrix shown in Fig. 6(a), indicating that static recrystallization was not so intense that an earlier shape fabric defined by phase boundaries could be erased. A few instances of coarser grains dispersed in the finer-grained matrix of the ultramylonitic gneisses are notable. We speculate that these grains mark locations where aggregates of finer grains with unpinned grain boundaries once existed, and are possibly examples of secondary recrystallization or exaggerated grain growth such as are found in annealed materials (e.g. Vernon, 1976; p. 145). Collectively, these observations suggest the grains in the ultramylonitic gneisses have coarsened through static recrystallization as much as was possible, but features such as phase boundary cusps and an earlier shape preferred orientation defined by phase boundaries persist to some degree.

Diffusion creep

The apparent mobility of phase boundaries in the Scituate mylonitic gneisses requires a process such as diffusion that is capable of redistributing matter. Diffusion creep is a deformation mechanism whereby strain is achieved by the transport of matter from areas of high stress to areas of low stress via either lattice diffusion (Nabarro-Herring creep) or grain boundary diffusion (Coble creep) (Poirier, 1985). The latter may be facilitated by the faster diffusion afforded by a grain boundary fluid, either aqueous or magmatic.

Gower & Simpson (1992) reviewed the literature on microstructural evidence for diffusion creep in experimental and natural studies, and enumerated the following features as indicative of this process: grain indentation, evidence for fine-scale dissolution and low dislocation densities, grain overgrowths, and truncation of compositional zoning by indenting grains. Many of these features are observed in the Scituate mylonitic gneisses studied here. There is abundant evidence for apparent grain indentation, particularly equant quartz grains apparently indenting microcline and plagioclase (Fig. 5c,d,f), and equant quartz grains apparently indenting and truncating zoned plagioclase (Fig. 5e). The greater apparent strength of quartz relative to feldspar should not be viewed in a purely mechanical sense (there is no evidence for internal deformation of feldspar grains where quartz indents them), but the observed relationships represent an apparent strength inversion compared to the relative strengths commonly observed in quartzo-feldspathic rocks deforming by dislocation creep (e.g. Tullis, 2002; also see Rosenberg & Stünitz, 2003). Thus this feature might serve as an distinctive characteristic of high temperature deformation accommodated by diffusion creep in quartzo-feldspathic gneisses.

Diffusion creep produces shape changes in grains that must be accommodated by local grain boundary sliding to avoid the formation of overlaps or voids (Poirier, 1985). Grain boundary sliding results in a microstructure composed of equant grains with an absence of a shape preferred orientation if there is a significant rotational component to the deformation, or one composed of inequant grains with a shape preferred orientation if a rotational component is weak or absent (e.g. Lapworth *et al*., 2002). An example of a possible grain boundary sliding relationship is observed in mixed-phase hornblende-rich aggregates (Fig. 4a), where hornblende occurs as dispersed inter-

stitial grains filling potential spaces between feldspar and quartz (Fig. 5b). The equant to sub-equant shapes of the quartz and feldspar grains and the weak shape preferred orientation are consistent with this interpretation. The hornblende grains shown in Fig. 5(b) exhibit a variety of lattice orientations (extinctions), indicating they do not represent a single hornblende grain that has grown around quartz and feldspar grains, making them partial inclusions. These textural relationships have several similarities to those reported by Kruse & Stünitz (1999) for hornblende in mafic mylonites of the Jotun nappe in the Scandinavian Caledonides, which were interpreted to reflect grain boundary sliding.

An important difference between the present example and many other natural examples of grain boundary sliding is grain size. A dominance of grain boundary sliding has been documented in naturally deformed rocks with much finer grain sizes (typically < 10 μm; Behrmann & Mainprice, 1987), although several studies have identified likely diffusion creep microstructures in naturally deformed high-temperature quartzo-feldspathic gneisses of similar grain size to the Scituate mylonitic gneisses (Gower & Simpson, 1992; Martelat *et al*., 1999; Zulauf *et al*., 2002; Scheuvens, 2002; Lapworth *et al*., 2002; Rosenberg & Stünitz, 2003).

The grain-size sensitivity of diffusion creep must be considered when invoking its operation in such coarse-grained rocks. Flow laws for diffusion creep display strain rates that vary with the inverse of the grain size raised to the second or third power, which characterize Nabarro-Herring or Coble creep, respectively (Poirier, 1985). Thus, there is a rapid drop-off in strain rate of diffusion creep with even modest increases in grain size. This factor appears evident in the Scituate mylonitic gneisses in the differing microstructures associated with coarse vs. fine quartz grains; the coarse grains show abundant evidence of dislocation creep (elongate grains with lobate grain boundaries and chessboard extinction) whereas the fine grains lack these features and show apparent indenting relationships to feldspar. This suggests dislocation creep and diffusion creep were competing deformational mechanisms among domains on the thin section scale (cf. Heilbronner & Bruhn, 1998; Kruse & Stünitz, 1999), and dominance varied locally with factors such as grain size and phase distribution.

Melt-enhanced diffusion creep

The rate of diffusion creep is enhanced by higher temperatures and/or increased solubility of mineral components in the grain boundary fluid, either aqueous or melt. Enhancement by a grain boundary fluid permits diffusion creep to operate at coarser grain sizes than otherwise would be possible. For example, Tullis & Yund (1991) demonstrated that the presence of aqueous fluid at feldspar grain boundaries so greatly enhanced diffusion rates that deformation progressed from cataclastic flow directly to diffusion creep in their experiments, completely bypassing the field for dislocation creep. Silicate melts have a much greater solubility than aqueous fluids for the components in silicate minerals such as feldspar and quartz, and therefore should be even more efficient in enhancing diffusion creep. Experimental studies in granitic (e.g. Dell'Angelo *et al*., 1987), olivine-basalt (e.g. Cooper & Kohlstedt, 1984), and analogue systems (Park & Means, 1996) confirm that the presence of intergranular melt considerably enhances the rate of diffusion creep and grain boundary sliding. We have presented independent evidence that deformation in the Scituate mylonitic gneisses occurred in the presence of local partial melts. The critical question here is whether such an enhancement would enable diffusion creep to become the dominant deformation mechanism in rocks as coarse grained as the Scituate mylonitic gneisses, and whether the operation of melt-enhanced diffusion creep can be recognized and confirmed in the microstructures.

Microstructural evidence for the presence of melt in naturally deformed high-grade gneisses is difficult to establish. Sawyer (2001) suggested a number of microstructures are indicative of the former existence of partial melt, including cuspate-shaped areas inferred to be crystallized melt surrounded by embayed grains, inferred melt pools with angular or blocky outlines due to crystal growth, rounded and corroded reactant minerals surrounded by crystallized melt, and inferred melt films along grain boundaries. With the exceptions noted above for the granitic lenses in the mylonitic gneisses studied here, unequivocal microstructural evidence for intergranular melt in the mylonitic gneisses was not observed. Unfortunately, microstructures associated with melt-present and melt-absent deformation at high temperature are generally similar at low melt fractions (e.g. see review of Rosenberg, 2001) and the criteria indicated above clearly include a degree of subjectivity. In fact, many of the cuspate/lobate and interstitial phase relationships recognized in this study can be interpreted either as the product of diffusion creep or crystallization from interstitial melt. For example, Marchildon & Brown (2002) reported microstructures of rounded, equant quartz grains against feldspar that resemble those reported here, and interpreted the feldspar shapes as reflecting the distribution of interstitial melt in the anatectic rocks they studied.

Thus, there remain considerable uncertainties in resolving the roles of diffusion creep and partial melting in producing the observed microstructures. It is emphasized, however, that these processes are not mutually exclusive, and the microstructures associated with each can develop simultaneously if melt is present during deformation.

The degree to which a melt wets grain boundaries has a critical influence on the strength of partially

molten aggregates. Studies in the olivine-basalt system indicate dramatic weakening once several percent melt is present, which is sufficient to at least partially wet grain boundaries due to the relatively small dihedral angle for olivine-melt and the effects of crystalline anisotropy (see review of Kohlstedt & Zimmerman, 1996). In granitic melt systems, somewhat larger mineral-melt dihedral angles appear to prevail (Jurewicz & Watson, 1984; Laporte *et al*., 1997; Gleason *et al*., 1999; Rosenberg & Riller, 2000) and therefore larger melt fractions will be required for grain boundaries to be partially wetted. There is some evidence, however, that dihedral angles for feldspar-fluid might decrease strongly under differential stress (Tullis *et al*., 1996) and thus wetting would occur at smaller melt fractions during deformation.

Due to these and other uncertainties, we cannot further evaluate whether the increase in grain boundary diffusion rates afforded by the presence of melt is sufficient to enable diffusion creep to operate at the grain scales (up to 500 μm), differential stress, and strain rate that characterized deformation of the Scituate mylonitic gneisses. Given recent studies that have attributed deformational microstructures in similarly coarse-grained, high-grade gneisses to diffusion-accommodated grain boundary sliding, even under melt-absent conditions (Kruse & Stünitz, 1999; Lapworth *et al*., 2002; Rosenberg & Stünitz, 2003), it seems likely that it could.

CONCLUSIONS AND TECTONIC IMPLICATIONS

The processes of dynamic recrystallization, static recrystallization, melt-enhanced diffusion creep, and diffusion–accommodated grain boundary sliding all appear to have played roles in producing the microstructures observed in the Scituate mylonitic gneisses. Melt-enhanced diffusion creep and diffusion-accommodated grain boundary sliding appear to be important processes in producing the high-energy microstructures, low internal lattice strain, and mixed phase distributions observed in the finer-grained matrix of the mylonitic gneisses and in the ultramylonitic gneisses. These processes were subordinate to dynamic recrystallization accompanying dislocation creep at coarser grain sizes, such as observed in coarse quartz grains with strong sub-grain development. Static recrystallization subsequently coarsened mineral grains with unpinned grain boundaries, and was important in producing low-energy grain boundary microstructures observed in monophase aggregates of microcline. Thus a combination of melt-enhanced diffusion creep and dynamic recrystallization/static recrystallization processes led to a microstructure characterized by the intimate coexistence of cuspate/lobate phase boundaries and straight to gently curved grain boundaries.

In rare instances, interstitial relationships mimicking melt pools appear to be preserved, and the isotopic, mineral assemblage and field observations on pegmatite–gneiss relationships leave little doubt that melts were present during deformation. The presence of partial melt during deformation is significant rheologically as melt enhances the rate of diffusion creep. Melts can play an important role in precipitating a switch from dislocation creep to diffusion creep as the dominant deformation mechanism (see Rosenberg & Berger, 2001), without the need to achieve an extremely fine recrystallized or neocrystallized grain size (cf. Stünitz & Tullis, 2001). Melt-enhanced diffusion creep thus has the potential to significantly weaken the crust at particular sites within a developing orogen (e.g. Scheuvens, 2002). Such weakening at deep crustal levels may provide an explanation for why a fairly coherent crustal block such as the Esmond–Dedham terrane became deformed and eventually truncated along a high-temperature shear zone.

A remaining issue is why strain localized within this zone of mylonitic gneisses bordering the Hope Valley shear zone. Observations in the gneissic but non-mylonitic rocks constituting most of the 10–15 km-thick deformed margin of the Esmond–Dedham terrane indicate that deformation occurred at similar high temperatures (e.g. chessboard extinction in quartz and the development of small-scale quartz-rich pegmatitic segregations are common). There is also some evidence for diffusion creep among finer grains (e.g. fine equant quartz indenting feldspar) but with a much less pronounced development than is observed in the mylonitic gneisses studied here. A significant difference between the gneisses and the mylonitic gneisses is that the former show extensive development of mantled feldspar porphyroclasts and other microstructures indicating an important role for dynamic recrystallization accompanying dislocation creep. Thus both dislocation creep and diffusion creep were active in rocks across this region, but diffusion creep appears to have accommodated a greater percentage of strain within the mylonitic zone than in the non-mylonitic gneisses outside of it.

The reason for the differences in dominance of dislocation vs. diffusion creep is unresolved, but given the sensitivity of diffusion creep to melt percentage and wetting properties (e.g. Tullis *et al*., 1996; Kohlstedt & Zimmerman, 1996), we suggest it might be related to the percentage of melt developed. The abundance of pegmatite appears greater in the zone of mylonitic gneisses than outside of it, supporting this suggestion. A significant metamorphic temperature gradient is not apparent across the area where these microstructural changes are noted, but metamorphic temperatures are expected to be strongly buffered once granite-minimum partial melt is present. Therefore differences in amount of partial melt generated are expected to be more a function of availability of heat energy and volatiles than simply the existence of a temperature gradient.

The contribution from diffusion creep to the total strain in the non-mylonitic gneisses, although relatively

small, is possibly quite significant. Even a small component of diffusion creep will cause a reduction in rock strength, which may have enabled the 10–15 km-thick zone of gneissic deformation (predominantly by dislocation creep) to develop concomitantly with the more highly strained (and weaker) mylonitic gneisses. Thus the field association of penetrative gneissic fabrics and small-scale pegmatitic/granitic segregations (cf. 'fluid relocation textures' of Hibbard, 1987) may represent a particular style of deformation that marks those locations in deep-seated orogens where small amounts of partial melts were generated within crystalline basement and diffusion creep began to contribute to strain.

ACKNOWLEDGEMENTS

We thank J. Tullis and M. Stipp for numerous discussions on the microstructures in these challenging rocks, and for thoughtful reviews of earlier versions of this manuscript. We benefited greatly from their insights. We also thank J. Selverstone for helpful discussions, and C. Holyoke and J. Schwartz for reviews of earlier versions. Detailed journal reviews by C. Rosenberg and R. Vernon and comments by journal editor M. Brown resulted in many improvements and are gratefully acknowledged. Support for this work was provided by a Brown University UTRA grant to SRG and NSF grant EAR-0001150 to LPG.

REFERENCES

Behrmann, J. H. & Mainprice, D., 1987. Deformation mechanisms in a high-temperature quartz-feldspar mylonite: evidence for superplastic flow in the lower continental crust. *Tectonophysics*, **140,** 297–305.

Cooper, R. F. & Kohlstedt, D. L., 1984. Solution-precipitation enhanced creep of partially molten olivine-basalt aggregates during hot pressing. *Tectonophysics*, **107,** 207–233.

Dallain, C., Schulmann, K. & Ledru, P., 1999. Textural evolution in the transition from subsolidus annealing to melting process, Velay Dome, French Massif Central. *Journal of Metamorphic Geology*, **17,** 61–74.

Day, H. W., Bowen, M. V. & Abraham, K., 1980. Precambrian (?) crystallization and Permian (?) metamorphism of hypersolvus granite in the Avalon terrane of Rhode Island. *Geological Society of America Bulletin*, **91,** 1669–1741.

Dell'Angelo, L. N., Tullis, J. & Yund, R. A., 1987. Transition from dislocation creep to melt-enhanced diffusion creep in fine grained granitic aggregates. *Tectonophysics*, **139,** 325–332.

Fliervoet, T. F., White, S. H. & Drury, M. R., 1997. Evidence for dominant grain boundary sliding deformation in greenschist- and amphibolite-grade polymineralic ultramylonites from the Redband Deformed Zone, Central Australia. *Journal of Structural Geology*, **19,** 1495–1520.

Flood, R. H. & Vernon, R. H., 1988. Microstructural evidence of orders of crystallization in granitoid rocks. *Lithos*, **21,** 237–245.

Getty, S. R. & Gromet, L. P., 1988. Alleghanian polyphase deformation of the Hope Valley Shear Zone, Southeastern New England. *Tectonics*, **7,** 1325–1338.

Gleason, G. C., Bruce, V. & Green, H. W., 1999. Experimental investigation of melt topology in partially molten quartzofeldspathic aggregates under hydrostatic and non-hydrostatic stress. *Journal of Metamorphic Geology*, **17,** 705–722.

Gower, R. J. W. & Simpson, C., 1992. Phase boundary mobility in naturally deformed, high-grade quartzofeldspathic rocks: evidence for diffusion creep. *Journal of Structural Geology*, **14,** 301–313.

Gromet, L. P., 1989. Avalonian terranes and late Paleozoic tectonism in southeastern New England: Constraints and Problems. In: *Terranes in the Circum-Atlantic Paleozoic Orogens, Special Paper, 230*, (eds Dallmeyer, R. D. & Keppie, J. D.), pp. 193–211. Geological Society of America, Boulder

Gromet, L. P., 1991. Direct dating of deformational fabrics. In: *Applications of Radiogenic Isotope Systems to Problems in Geology, Short Course Handbook, 19*, (eds Heaman, L. & Ludden, J. N.), pp. 167–189. Mineralogical Association of Canada, Ottawa.

Gromet, L. P., Getty, S. R. & Whitehead, E. K., 1998. Late Paleozoic orogeny in southeastern New England: a mid-crustal view. In: *Guidebook to Fieldtrips in Rhode Island and Adjacent Regions of Connecticut and Massachusetts* (ed. D. Murray), 1998 New England Intercollegiate Geological Conference. University of Rhode Island, Kingston, RI, Chapter B2.

Heilbronner, R. & Bruhn, D., 1998. The influence of three-dimensional grain size distributions on the rheology of polyphase rocks. *Journal of Structural Geology*, **20,** 695–705.

Hermes, O. D., Gromet, L. P. & Murray, D. P., 1994. Bedrock Geologic Map of Rhode Island. *Rhode Island Map Series No 1, Office of the State Geologist*. University of Rhode Island, Kingston.

Hermes, O. D. & Zartman, R. E., 1985. Late Proterozoic and Devonian plutonic terrane within the Avalon zone of Rhode Island. *Geologic Society of America Bulletin*, **96,** 272–282.

Hibbard, M. J., 1979. Myrmekite as a marker between preaqueous and postaqueous phase saturation in granitic systems. *Geologic Society of America Bulletin*, **90,** 1047–1062.

Hibbard, M. J., 1987. Deformation of incompletely crystallized magma systems: granitic gneisses and their tectonic implications. *Journal of Geology*, **95,** 543–561.

Hirth, G. & Tullis, J., 1992. Dislocation creep regimes in quartz aggregates. *Journal of Structural Geology*, **14,** 145–159.

Holtzman, B. K., Groebner, N. J., Zimmerman, M. E., Ginsberg, S. B. & Kohlstedt, D. L., 2003. Stress-driven melt segregation in partially molten rocks. *Geochemistry Geophysics Geosystems*, **4**.

Jurewicz, S. R. & Watson, E. B., 1984. Distribution of partial melt in a felsic system: the importance of surface energy. *Contributions to Mineralogy and Petrology*, **85,** 25–29.

Kohlstedt, D. L. & Zimmerman, M. E., 1996. Rheology of partially molten mantle rocks. *Annual Reviews of Earth and Planetary Sciences*, **24,** 41–62.

Kruhl, J. H., 1996. Prism- and basal-plane parallel subgrain boundaries in quartz: a microstructural geothermobarometer. *Journal of Metamorphic Geology*, **14,** 581–589.

Kruse, R. & Stünitz, H., 1999. Deformation mechanisms and phase distribution in mafic high-temperature mylonites from the Jotun Nappe, southern Norway. *Tectonophysics*, **303,** 223–249.

Laporte, D., Rapaille, C. & Provost, A., 1997. Wetting angles, equilibrium melt geometry, and the permeability threshold of partially molten crustal protoliths. In: *Granite: from Segregation of Melt to Emplacement Fabrics* (eds Bouchez, J. L., Hutton, D. H., & Stephens, W. E.), pp. 31–54. Kluwer Academic Press, Amsterdam.

Lapworth, T., Wheeler, J. & Prior, D. J., 2002. The deformation of plagioclase investigated using electron backscatter diffraction crystallographic preferred orientation data. *Journal of Structural Geology*, **24,** 387–399.

Ludwig, K. R., 2001. Isoplot/Ex: A geochronological toolkit for Microsoft Excel. *Special Publication, 1a*. Berkeley Geochronological Center, Berkeley.

Mainprice, D., Bouchez, J., Blumenfeld, P. & Tubia, J. M., 1986. Dominant c slip in naturally deformed quartz: Implications for dramatic plastic softening at high temperature. *Berkeley Geology*, **14,** 819–822.

Marchildon, N. & Brown, M., 2002. Grain-scale melt distribution in two contact aureole rocks: implications for controls on melt localization and deformation. *Journal of Metamorphic Geology*, **20,** 381–396.

Marchildon, N. & Brown, M., 2003. Spatial distribution of melt-bearing structures in anatectic rocks from Southern Brittany, France: implications for melt transfer at grain- to orogen scale. *Tectonophysics*, **364,** 215–235.

Martelat, J., Schulmann, K., Lardeaux, J., Nicollet, C. & Cardon, H., 1999. Granulite microfabrics and deformation mechanisms in southern Madagascar. *Journal of Structural Geology*, **21,** 671–687.

O'Hara, K. & Gromet, L. P., 1985. Two distinct late Precambrian (Avalonian) terranes in southeastern New England and their late Paleozoic juxtaposition. *American Journal of Science*, **285,** 673–709.

Park, Y. & Means, W. D., 1996. Direct observation of deformation processes in crystal mushes. *Journal of Structural Geology*, **18,** 847–858.

Poirier, J., 1985. *Creep of Crystals*. Cambridge University Press, Cambridge.

Quinn, A. W., 1971. Bedrock Geology of Rhode Island. *United States Geological Survey Bulletin*, **1295**.

Rosenberg, C. L., 2001. Deformation of partially molten granite: a review and comparison of experimental and field investigations. *International Journal of Earth Sciences*, **90,** 60–76.

?twb = .25w > Rosenberg, C. L. & Berger, A., 2001. Syntectonic melt pathways in granite, and melt-induced transition in deformation mechanisms. *Physics and Chemistry of the Earth, Part A*, **26,** 287–293.

Rosenberg, C. L. & Riller, U., 2000. Partial-melt topology in statically and dynamically recrystallized granite. *Geology*, **28,** 7–10.

Rosenberg, C. L. & Stünitz, H., 2003. Deformation and recrystallization of plagioclase along a temperature gradient: an example from the Bergell tonalite. *Journal of Structural Geology*, **25,** 389–408.

Sawyer, E. W., 2001. Melt segregation in the continental crust: distribution and movement of melt in anatectic rocks. *Journal of Metamorphic Geology*, **19,** 291–309.

Scheuvens, D., 2002. Metamorphism and microstructures along a high-temperature metamorphic field gradient: the north–eastern boundary of the Královsk'y hvozd unit (Bohemian Massif, Czech Republic). *Journal of Metamorphic Geology*, **20,** 413–428.

Simpson, C. & Wintsch, R. P., 1989. Evidence for deformation-induced K-feldspar replacement by myrmekite. *Journal of Metamorphic Geology*, **7,** 261–275.

Stipp, M., Stünitz, H., Heilbronner, R. & Schmid, S. M., 2002. The eastern Tonale fault zone: a 'natural laboratory' for crystal plastic deformation of quartz over a temperature range from 250 to 700 °C. *Journal of Structural Geology*, **24,** 1861–1884.

Stünitz, H. & FitzGerald, J. D., 1993. Deformation of granitoids at low metamorphic grade II: Granular flow in albite-rich mylonites. *Tectonophysics*, **221,** 299–324.

Stünitz, H. & Tullis, J., 2001. Weakening and strain localization produced by syn-deformational reaction of plagioclase. *International Journal of Earth Sciences*, **90,** 136–148.

Tullis, J., 1990. Experimental studies of deformation mechanisms and microstructures in quartzo-feldspathic rocks. In: *Deformation Processes in Minerals, Ceramics and Rocks* (eds Barber, D. J. & Meredith, P. G.), pp. 190–227. Unwin-Hyman, London.

Tullis, J., 2002. Deformation of granitic rocks: experimental studies and natural examples. In: *Plastic Deformation of Minerals and Rocks, Reviews in Mineralogy and Geochemistry, 51*. (eds S. Karato & H. Wenk), pp. 51–95. Mineralogical Society of America, Washington DC.

Tullis, J. & Yund, R. A., 1985. Dynamic recrystallization of feldspar: a mechanism for ductile shear zone formation. *Geology*, **13,** 238–241.

Tullis, J., Yund, R. & Farver, J., 1996. Deformation-enhanced fluid distribution in feldspar aggregates and implications for ductile shear zones. *Geology*, **24,** 63–66.

Tullis. J. & Yund, R. A., 1991. Diffusion creep in feldspar aggregates—experimental evidence. *Journal of Structural Geology*, **13,** 987–1000.

Vernon, R. H., 1968. Microstructures of high-grade metamorphic rocks at Broken Hill, Australia. *Journal of Petrology*, **9,** 1–22.

Vernon, R. H., 1976. *Metamorphic Processes*. Wiley, New York.

Vernon, R. H. & Collins, W. J., 1988. Igneous microstructures in migmatites. *Geology*, **16,** 1126–1129.

Zen, E.-an, 1983. Exotic terranes in the New England Appalachians – limits, candidates, and ages: A speculative essay. In: *Contributions to the Tectonic and Geophysics of Mountain Chains, Memoir, 158*, (eds R. D. Hatcher, H. Williams & I. Zietz), pp. 55–81. Geological Society of America, Boulder

Zulauf, G., Dorr, W., Fiala, J., Kotkova, J., Maluski, H. & Valverde-Vaquero, P., 2002. Evidence for high-temperature diffusional creep preserved by rapid cooling of lower crust (North Bohemian shear zone, Czech Republic). *Terra Nova*, **14,** 343–354.

Received 18 May 2003; revision accepted 1 October 2003.